Supplemental Information

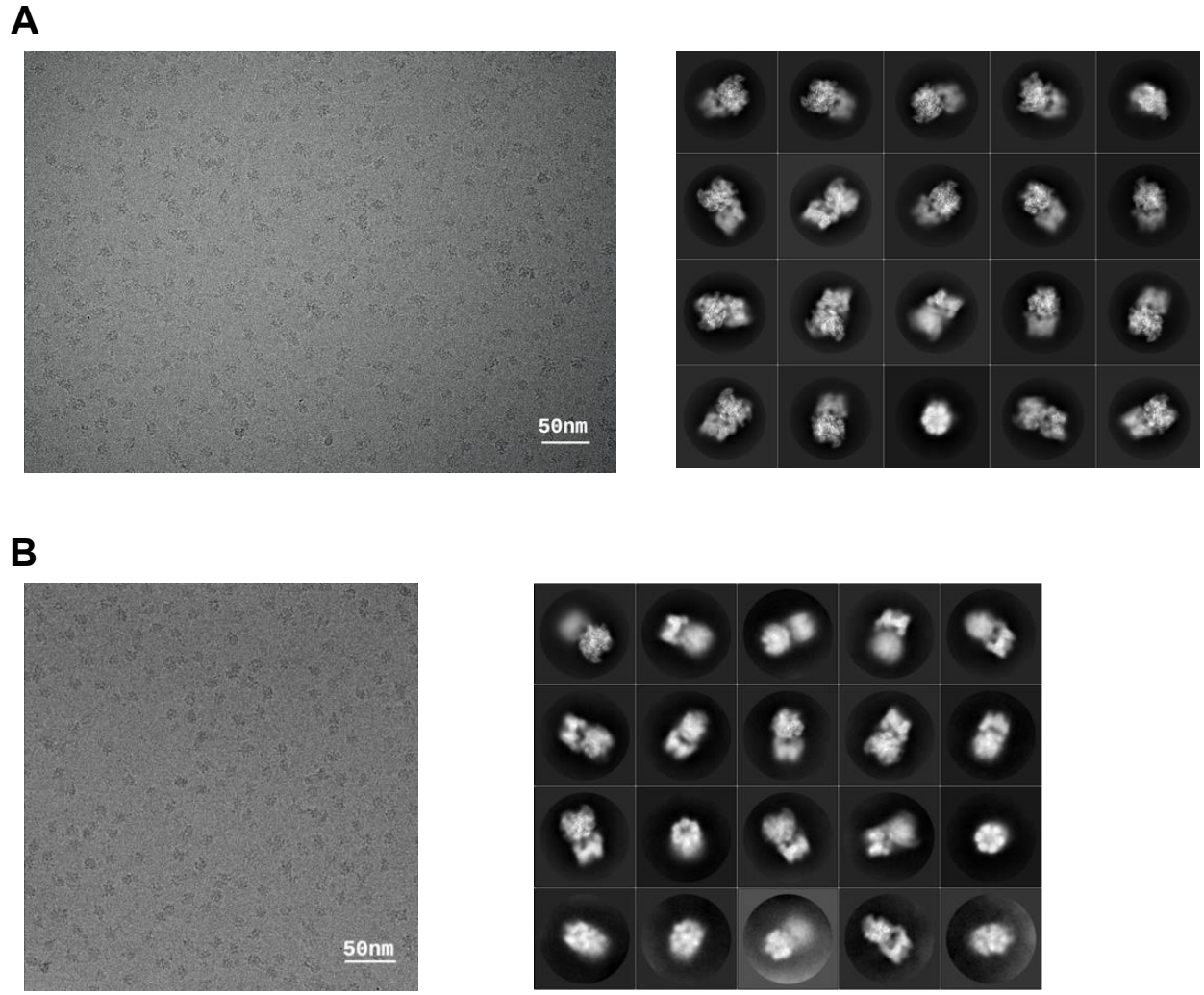

Figure S1. Cryo-EM Imaging of PTC60 and PTC18, Related to Figures 2 and 3.
(A) Selected micrograph (left panel) and averages of the 20 most populated classes from the second 2D classification (right panel) of PTC60 in vitreous ice. The spherical mask diameter is 320 Å.
(B) Selected micrograph (left panel) and averages of the 20 most populated classes from the second 2D classification (right panel) of PTC18 in vitreous ice. The spherical mask diameter is 320 Å.

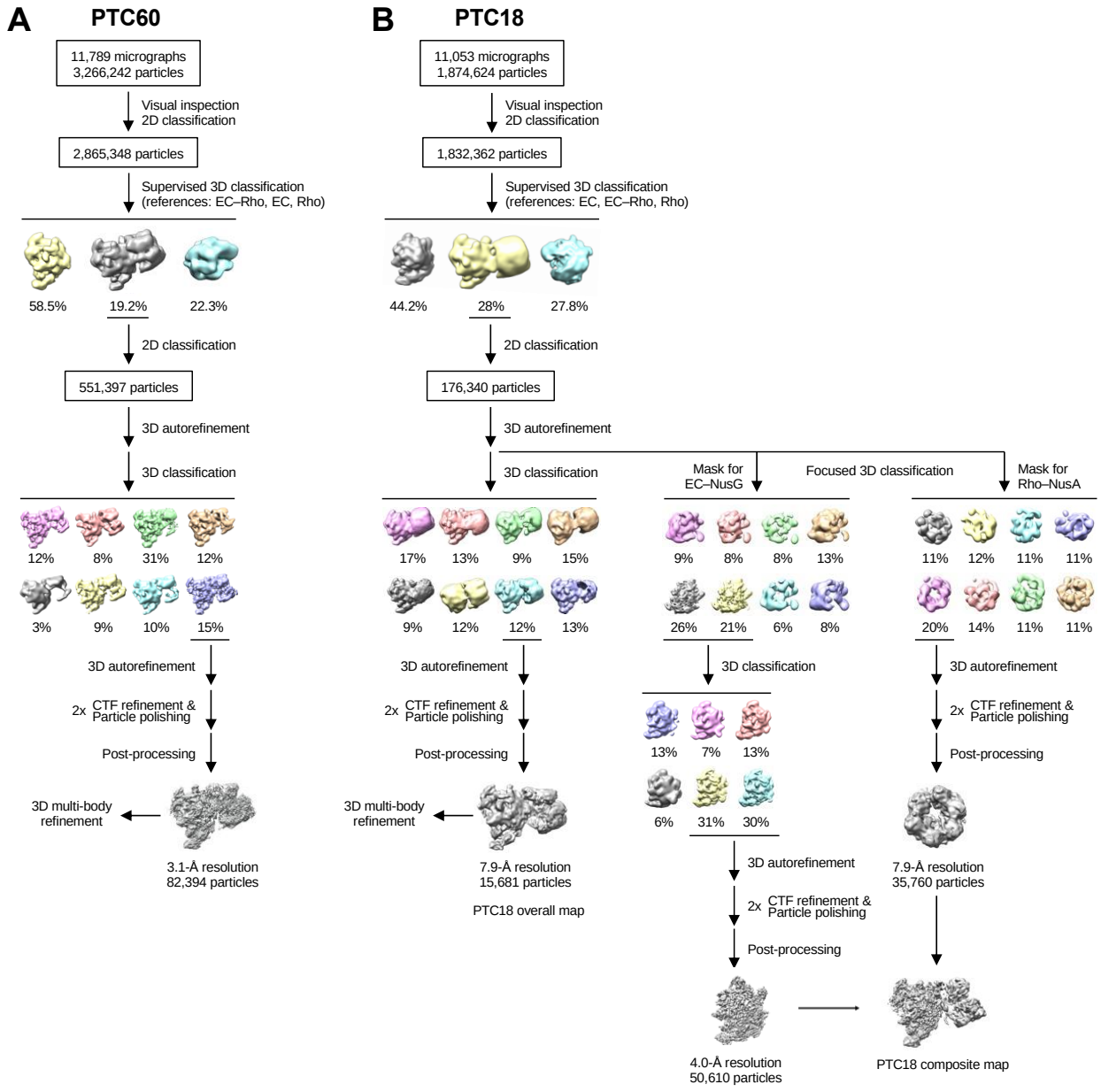

Figure S2. Data-processing Workflow for the Cryo-EM Datasets of PTC60 and PTC18, Related to Figures 2 and 3.

(A) Flowchart showing the image-processing pipeline used for the cryo-EM dataset of PTC60, yielding the final density map at 3.1-Å nominal resolution. See Star Methods for details.

(B) Flowchart showing the same image-processing pipeline used for the cryo-EM dataset of PTC60, yielding the final "overall" density map for PTC18 at 7.9-Å nominal resolution (left arm). In parallel, focused classifications and refinements were performed for the EC–NusG density (middle arm) and the Rho–NusA density, yielding final density maps at nominal resolutions of 4.0 Å and 7.9 Å, respectively, which were combined into the "composite" density map for PTC18.

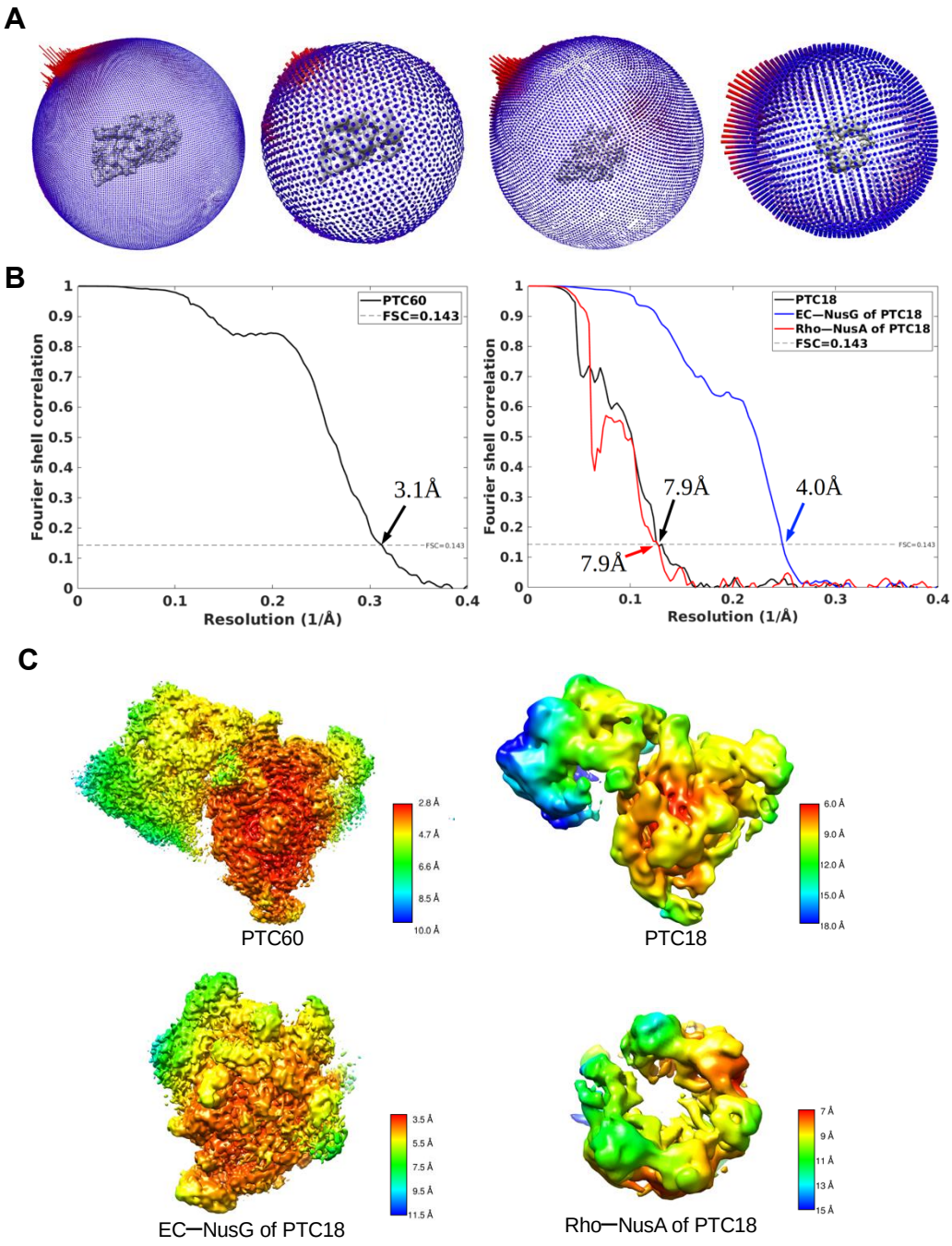

Figure S3. Quality Assessment of the PTC60 and PTC18 Maps, Related to Figures 2 and 3.
(A) Angular distribution for the particle projections used for the final PTC60 map, the PTC18 overall map, and the density maps for EC–NusG and Rho–NusA of PTC18 obtained by focused classification and refinement.
(B) left panel: Fourier shell correlation (FSC) curves for PTC60. The FSC curves were calculated by comparing two independently determined half-maps. The dotted line represents the FSC = 0.143 cutoff, which indicates a nominal resolution of 3.1 Å for the PTC60 map. Right panel: FSC curves for PTC18. The dotted line represents the FSC = 0.143 cutoff, which indicates a nominal resolution of 7.9 Å for the PTC18 overall map, and 4.0 Å and 7.9 Å for the EC–NusG and Rho–NusA densities, respectively, obtained by focused classification and refinement.
(C) Local resolution of the PTC60 map (upper left panel), the PTC18 overall map (upper right panel), and the density maps for EC–NusG (lower left panel) and Rho–NusA of PTC18 (lower right panel) obtained by focused classification and refinement.

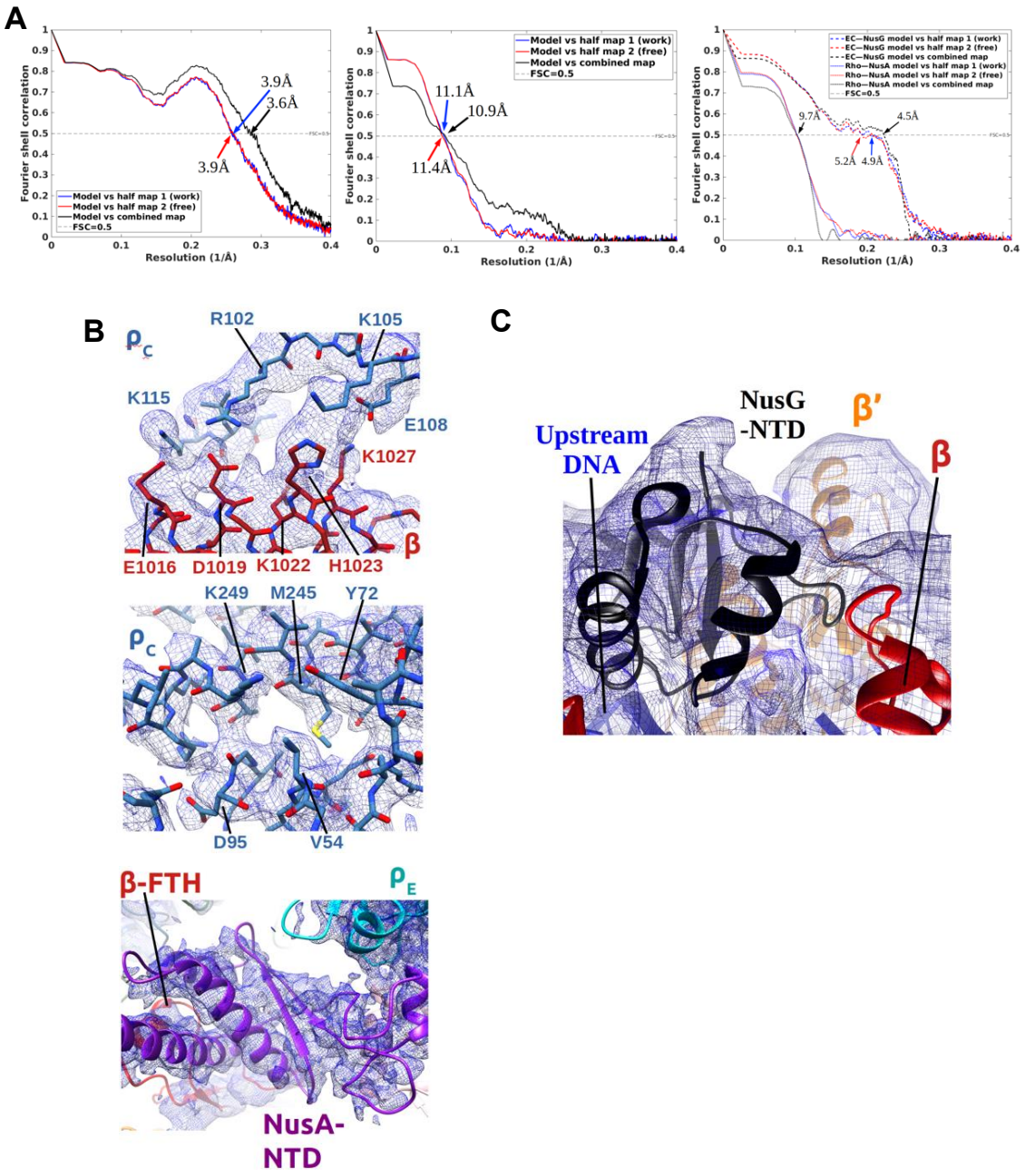

Figure S4. Quality Assessment of the PTC60 and PTC18 Models, Related to Figures 2, 3 and 4.
(A) FSC curves calculated between the refined structure and the half map used for refinement (work), the half map not used for refinement (free), and the combined map for PTC60 (left panel) and PTC18 (middle and right panels). FSC curves in the middle panel were calculated using the entire PTC18 model and the PTC18 overall map. FSC curves in the right panel were calculated using 1) the EC and NusG models of PTC18 and the EC–NusG map obtained by focused classification and refinement and 2) the Rho and NusA models of PTC18 and the Rho–NusA map obtained by focused classification and refinement.
(B) Representative regions of the cryo-EM map and model of PTC60. Upper panel: Cryo-EM density (blue mesh) and model for the β—ρ_C interactions. Middle panel: Cryo-EM density (blue mesh) and model for ρ_C. Lower panel: Cryo-EM density (blue mesh, filtered to the local resolution) for the NusA-NTD and the interacting regions.
(C) Representative region of the PTC18 composite map with the fitted model. Cryo-EM density (blue mesh, filtered to the local resolution) and model for the NusG-NTD, upstream duplex DNA, RNAP β and β' subunit.

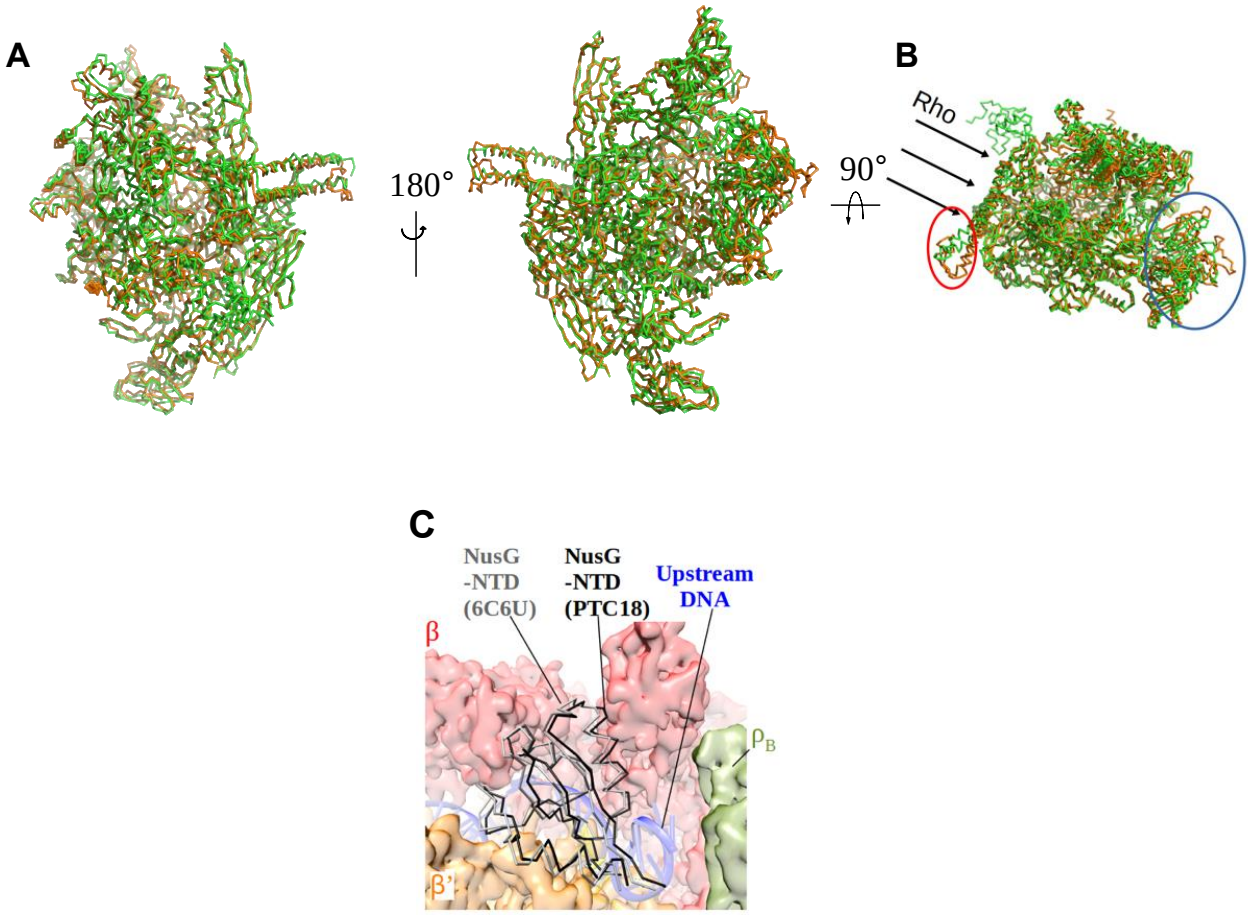

Figure S5. Structural Comparisons, Related to Figures 2, 3 and 4.
(A) Superimposition of RNAP in the *E. coli* EC (orange, PDB: 6ALH) and in PTC60 (green). Both models are shown as Cα models.
(B) Orientation of RNAP relative to bound Rho in PTC60. Arrows indicate the direction from which Rho binds to RNAP in the PTC60 structure. The red oval indicates the region in which major conformational changes occur in RNAP upon Rho binding. The blue oval indicates the flexible β' I3 region.
(C) The previously determined structure of NusG-NTD bound to *E. coli* EC (PDB: 6C6U) is superimposed onto the NusG-NTD in PTC18 (the EC–NusG structure was aligned with the PTC18 structure based on the RNAP β and β' subunits, resulting in an RMSD of 1.456 Å for the 98 corresponding Cα atoms of NusG-NTD. NusG-NTD in PTC18 is shown in black and NusG-NTD as part of the EC–NusG complex in gray.

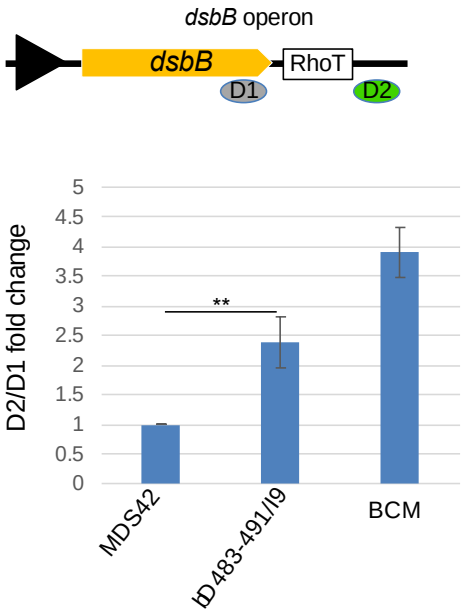

Figure S6. Chromosomal Δβ483-491/I9 Deletions in RNAP Compromise Rho-dependent Termination *in vivo*, Related to Figure 3. Upper panel: Schematic diagram of the chromosome-based Rho-dependent terminator reporter. P (black triangle) indicates the native promoter, and RhoT is a prominent Rho/NusG-dependent terminator (Dar and Sorek, 2018). D1 and D2 indicate the locations of qRT-PCR amplicons. Lower panel: fold changes in Rho-dependent termination for *E. coli* MDS42 strains containing the Δβ483-491/I9 double deletion. BCM is bicyclomycin (5 µg/ml), which was used as positive control. qRT-PCR data are shown in fold changes of the D2/D1 amplicon signal; data from four independent experiments are presented as the means ± SEM; **P < 0.01.

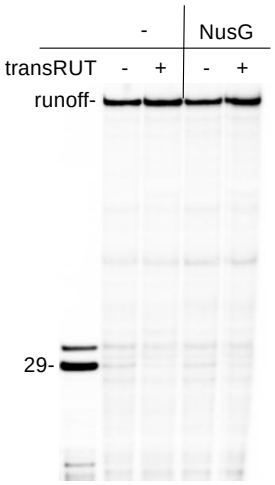

Figure S7. transRUT Does Not Induce Termination Without Rho, Related to Figure 6. EC29 was prepared and chased as in Figure 6B (lane 7), except that Rho was omitted from the chase reaction.

Table S1. List of *In-vivo* Crosslinking Sites between RNAP, Rho, NusA and NusG When Rho-dependent Termination Is Inhibited by Bicyclomycin, Related to Figure 2.

Components	Cross-linking sites	Scores
Rho−RNAP	Rho(1)−RpoB(1032)[#(32.5)]	8.702E-05
	Rho(123)−RpoB(1078)[#(79.6)]	1.470E-03
Rho−NusA	NusA(447)−Rho(115)	1.007E-05
	NusA(447)−Rho(123)	1.007E-05
Rho−NusG	NusG(106)−Rho(257)	4.82E-02
NusA−RNAP	NusA(3)−RpoB(900) [#(20.3)]	7.93E-10
	NusA(16)−RpoB(909) [#(24.0)]	3.50E-09
	NusA(37)−RpoB(909)[#(17.6)]	4.35E-10
	NusA(38)−RpoB(909) [#(17.3)]	8.76E-11
	NusA(111)−RpoB(890) [#(16.7)]	4.34E-06
	NusA(111)−RpoB(900) [#(17.6)]	2.45E-08
	NusA(111)−RpoB(909) [#(10.4)]	5.81E-11
	NusA(111)−RpoC(66) [#(25.6)]	2.22E-06
	NusA(111)−RpoC(395) [#(33.1)]	5.98E-10
NusG−RNAP	NusG(125) −RpoC(40)	6.19E-08

Filtered for FDR(<5%), e-value (<1.0E-3), pLink2 score (<1.0E-2), and abundance (PSMs≥5)

[#] Cross-linking sites that shown in Figure 2D. The following numbers in parentheses represent distance between two alpha carbons (in Å).

Table S2. Cryo-EM Data Collection and Refinement Statistics, Related to Figures 2 and 3.

Structure	PTC60	PTC18
Model (PDB)	6XAS	6XAV
Density map (EMDB)	22114	22115
Data Collection and Processing		
Microscope	FEI Titan Krios	FEI Titan Krios
Voltage (kV)	300	300
Detector	K3 summit	K2 summit
Electron exposure ($e^-/Å^2$)	50	68
Defocus range (μm)	0.8-1.8	1.0-2.5
Data collection mode	Super-resolution	Counting
Pixel size	1.078	1.048
Symmetry imposed	C1	C1
Initial particle images (No.)	551,397	176,340
Final particle images (No.)	82,394	15,681
Map resolution (Å) **(FSC threshold)**	3.1/3.8 (0.143/0.5)	7.9/10.0 (0.143/0.5)
Refinement		
Map sharpening B factor ($Å^2$)	-51.80	-40.40
RMSD		
Bond lengths (Å) (# > 4σ)	0.002 (0)	0.002 (0)
Bond angles (°) (# > 4σ)	0.473 (1)	0.447 (1)
Ramachandran		
Favored (%)	97.80	97.48
Allowed (%)	2.19	2.51
Outliers (%)	0.02	0.01
MolProbity Validation		
Clash score	4.90	6.75
Poor rotamer (%)	1.49	1.59
Overall score	1.43	1.61

Table S3. RMSD Calculation, Related to Figure S5.

Structural module	Residue No.	RMSD (# of Cα)
Central Domains*	α1: 10-158, 167-234 α2: 16-52, 179-232 β: 3-40, 130-225, 344-890, 913-933, 1041-1318 β': 16-35, 95-142, 209-645, 765-933, 1136-1151, 1215-1373	1.116 Å (1,832)
Entire RNAP	α1: 7-158, 167-234 α2: 4-158, 170-232 β: 3-890, 913-982, 1002-1341 β': 16-933, 946-1126, 1136-1373 ω: 2-56	1.454 Å (2,615)
NusG-NTD	Residue: 6-48, 63-117	1.456 Å (98)

*Structures were aligned by Central domains before RMSD calculation.

Table S4. List of *In-vitro* Cross-linking Sites between RNAP, Rho, NusA and NusG in PTC18, Related to Figure 4.

Components	XL sites	Score	XL site	Score	XL sites	Score	XL sites	Score
Rho−RNAP	Rho(115) −RpoB(115)#(17.9)	9.29E-003	Rho(115)−RpoA(297)	8.14E-004	Rho(123)−RpoB(331)	2.09E-002	Rho(40)−RpoB(909)	2.16E-001
	Rho(44)−RpoB(991)#(32.9)	4.55E-005	Rho(40)−RpoC(2)	2.38E-004	Rho(224)−RpoA(297)	3.97E-002	Rho(40)−RpoC(1297)	4.31E-003
	Rho(283)−RpoB(900) #(23.8)	8.11E-008	Rho(385)−RpoB(1032)	7.09E-003	Rho(283)−RpoB(1032)	9.38E-002	Rho(44)−RpoA(297)	1.10E-001
	Rho(115)−RpoA(291) #(16.2)	1.69E-008	Rho(105)−RpoA(291)	4.26E-003	Rho(283)−RpoC(87)	3.25E-005	Rho(44)−RpoA(298)	7.60E-004
	Rho(40)−RpoA(297) #(18.7)	2.59E-003	Rho(105)−RpoC(39)	6.01E-002	Rho(40)−RpoB(900)	1.84E-004		
	Rho(40)−RpoB(991) #(33.0)	9.22E-004	Rho(115)−RpoA(298)	1.23E-006	Rho(100)−RpoA(298)	6.68E-004		
	Rho(105)−RpoB(1027) #(12.2)	3.28E-005	Rho(283)−RpoB(909)	2.34E-004	Rho(224)−RpoA(298)	1.20E-003		
	Rho(40)−RpoA(298) #(19.9)	1.11E-004	Rho(105)−RpoB(1133)	2.96E-002	Rho(283)−RpoC(296)	2.29E-001		
	Rho(100)−RpoA(291) #(18.7)	4.57E-003	Rho(123)−RpoB(988)	1.03E-001	Rho(283)−RpoC(531)	3.19E-002		
	Rho(40)−RpoA(291) #(21.2)	6.26E-005	Rho(105)−RpoC(40)	1.32E-003	Rho(367)−RpoB(1027)	9.02E-003		
Rho−NusA	NusA(52) −Rho(283) #(15.4)	2.07E-011	NusA(224)−Rho(123)	9.70E-004	NusA(201)−Rho(105)	1.21E-003	NusA(411)−Rho(115)	3.45E-006
	NusA(239)−Rho(123)	1.16E-002	NusA(52)−Rho(40) #(38.0)	2.31E-010	NusA(22)−Rho(181) #(37.6)	3.66E-004	NusA(16)−Rho(283)	2.68E-003
	NusA(224)−Rho(100)	8.61E-006	NusA(16)−Rho(181) #(30.6)	1.88E-002	NusA(239)−Rho(115)	2.82E-003	NusA(52)−Rho(181)	7.09E-003
	NusA(52)−Rho(123) #(42.7)	2.53E-006	NusA(22)−Rho(105) #(21.9)	1.86E-002	NusA(52)−Rho(115)	2.38E-006	NusA(52)−Rho(44)	3.58E-002
Rho−NusG	NusG(125) −Rho(115)*	7.82E-010	NusG(125)−Rho(100)*	1.75E-002	NusG(125)−Rho(105)*	1.70E-004	NusG(121)−Rho(40)	4.56E-002
	NusG(121)−Rho(115)*	3.97E-003	NusG(121)−Rho(123)*	2.44E-002	NusG(125)−Rho(40)	4.94E-004	NusG(121)−Rho(44)	1.83E-001
	NusG(125)−Rho(123)*	5.31E-004	NusG(121)−Rho(100)*	2.65E-002	NusG(106)−Rho(181)	4.35E-002		
NusA−RNAP	NusA(111) −RpoC(66) #(22.1)	8.36E-003	NusA(144)−RpoC(87) #(21.7)	3.71E-10	NusA(16)−RpoC(2)	1.10E-003	NusA(429) −RpoC(9)	5.41E-002
	NusA(22)−RpoB(900) #(26.0)	1.22E-006	NusA(144)−RpoC(66) #(25.9)	3.37E-09	NusA(411)−RpoB(844)	1.43E-003	NusA(429)−RpoC(321)	5.44E-002
	NusA(16)−RpoC(66) #(33.5)	1.61E-002	NusA(144)−RpoC(1306)	1.43E-07	NusA(16)−RpoC(9)	1.46E-003	NusA(429)−RpoA(297)	5.89E-002
	NusA(22)−RpoC(87) #(34.0)	7.49E-006	NusA(144)−RpoB(900)	1.03E-05	NusA(111) −RpoC(395)	1.78E-003	NusA(111)−RpoB(890)	6.84E-003
	NusA(16)−RpoB(900) #(24.7)	3.20E-005	NusA(144)−RpoC(96)	1.45E-04	NusA(111)−RpoB(900)	4.62E-002	NusA(22)−RpoC(50)	7.02E-004
	NusA(52)−RpoC(87) #(41.0)	9.21E-006	NusA(16)−RpoB(909)	2.87E-004	NusA(16)−RpoC(50)	3.01E-003	NusA(201)−RpoB(844)	8.05E-003
	NusA(111)−RpoB(914) #(16.4)	1.36E-002	NusA(38)−RpoB(909)	4.36E-005	NusA(411)−RpoC(9)	1.29E-002	NusA(38)−RpoA(298)	1.37E-002
	NusA(429)−RpoB(844)	3.18E-005	NusA(143)−RpoB(900)	5.89E-003	NusA(111)−RpoB(909)	6.88E-002	NusA(37)−RpoB(909)	2.66E-002
NusG−RNAP	NusG(125)−RpoC(40)	1.39E-008	NusG(155)−RpoC(50)*	2.09E-001	NusG(121)−RpoC(40)	2.90E-002	NusG(125)−RpoC(39)	1.67E-003
	NusG(155)−RpoC(40)*	2.43E-010	NusG(125)−RpoC(50)	2.19E-002	NusG(159)−RpoC(50)*	1.03E-002	NusG(125)−RpoC(87)	3.64E-001

Filtered for FDR(<5%), e-value (<1.0E-3), pLink2 score (<1.0E-2), and abundance (PSMs≥5)

#Cross-linking sites that shown in Figure 4A. The following numbers in parentheses represent distance between two alpha carbons (in Å).

*Cross-linking sites that used to facilitate NusG-CTD docking in Figure 4B.

Table S5. DNA and RNA Sequences in the Assays, Related to STAR Methods.

Name	Sequence

Template 1 (Promoter region is shown in dashed underline; Transcribing region is shown in uppercase.)	tccagatccc gaaaatttat caaaaagagt attgacttaa agtctaacct ataggatact tacagcc ATCGAGAGGG CCACGGCGAA CAGCCAACCT AATCGACACC GGGGTCCGGG ATCTGGATCT GGATCGCGAA TTCCAGGCCT GCTGGTAATC TTTGGATCCC CGGGTACCGA GCTCGAATTC ACTGGCCGTC GTTTTACAAC GTCGTGACTG GGAAAACCCT GGCG
RUT81 RNA	**CCCUCAACGACCCCUUCCUUCUCCCCAUCGCUACCUCAUAUCCGCAC CUCCUCAAACGCUACCUCGACCAGCCUCCCCUCCC**
qPCR target region of the pVE-rut81-GFP plasmid. (Constitutive campylobacter promoter is shown in dashed underline; Transcribing region is shown in uppercase; Rut81 sequence is shown in bold italic uppercase; GFP gene is shown in bold uppercase; Positions of the qPCR primer regions are underlined.)	ggaattggggatcggaagcttgcatgcctgcaggtcgactctagaggatccgttattttaagtcttagtttagttttttggtata attagaattcATCGAGAGGGCCACGGCGAACAGCCAACCTAATCGACACCGGGG TCCGGGATCTGGATCTGGATCGCGATTTACAGGCCTGCTGGTAATCTTTGG ATCCCCGGGTACCGAGCTCGAATTCACTGGCCGTCGTTTTACAACGTCGTG ACTGGGAAAACCCTCTCGAG***CCCTCAACGACCCCTTCCTTCTCCCCATCGC TACCTCATATCCGCACCTCCTCAAACGCTACCTCGACCAGCCTCCCTCCC***GA GCTCTAATTGCTAAATTCGGCTTATTCCCTAACTAACTAAAGATTAACTTT ATAAGGAGGAAAAACAT**ATGAGTAAAGGAGAAGAACTTTTCACTGGAG TTGTCCCAATTCTTGTTGAATTAGATGGTGATGTTAATGGGCACAAAT TTTCTGTCAGTGGAGAGGGTGAAGGTGATGCAACATACGGAAAACTT ACCCTTAAATTTATTTGCACTACTGGAAAACTACCTGTTCCATGGCCA ACACTTGTCACTACTTTGACTTATGGTGTTCAATGCTTTTCAAGATAC CCAGATCATATGAAACGGCATGACTTTTTCAAGAGTGCCATGCCCGA AGGTTATGTACAGGAAAGAACTATATTTTTCAAAGATGACGGGAACTA TAAGACACGTGCTGAAGTCAAGTTTGAAGGTGATACACTTGTTAATAG AATCGAGTTAAAAGGTATTGATTTTAAAGAAGATGGAAACATTCTTGG ACACAAGTTGGAATACAACTATAACTCACACAATGTATACATCATGGC AGACAAACAAAAGAATGGAATCAAAGTTAACTTCAAAATTAGACACAA CATTGAAGATGGAAGCGTTCAACTAGCAGACCATTATCAACAAAATAC TCCAATTGGCGATGGCCCTGTCCTTTTACCAGACAACCATTACCTGTC CACACAATCTGCCCTTTCGAAAGATCCCAACGAAAAGAGAGACCACA TGGTCCTTCTTGAGTTTGTAACAGCTGCTGGGATTACACATGGCATGG ATGAACTATACAAATAG**
T7A1-Trpt1 (Promoter region is shown in dashed underline; Transcribing region is shown in uppercase; Natural RUT site is shown in bold uppercase.)	tccagatccc gaaaatttat caaaaagagt attgacttaa agtctaacct ataggatact tacagcc ATCGAGAGGGACACGGCGAAGGCGGCATTTTAACTTTCTTTAATGAAGCC GGAAAAATCCTAAATTCATTTAATATTTATCTTTTTACCGTTTCGCTTACCC CGGTCGAACGT**CAACTTACGTCATTTTTCCGCCCAACAGTAATATAATC AAACAAATTAATCCCGCAACATAACACCAGTAAAATCAATAATTTTCT CTAAGTCACTTATTCCTCA**GGTAATTGTTAATATATCCAGAATGTTCCTC AAAATATATTTTCCCTCTATCTTCTCGTTGCGCTTAATTTGACTAATTCTCA TTAGCGACTAATTTTAATGAGTGTCGACACACAACACTCATATTAATGAA ACAATGCAACGCAACGGGAGAAATAACATGGCCGAACATCGTGGTGGTT CAGGAAATTTCGCCGAAGACCGTGAGAAGGCATCCGACGCAGGCCGTAA AGGCGGTCAGCATAGCGGCGGTAATTTTAAAAATGATCCGCAACGCGCAT CTGAAGCGGGTAAAAAAGGCGGTCAACAAAGCGGTGGTAATAAATCAGG CAAATCCTG

Movie S1. Motions Corresponding to the First Three Eigenvectors from the Multibody Refinement of the PTC60 Dataset. Eigenvector #1 accounts for 24.6% of the total variance in

the dataset, eigenvector #2 for 22.7%, and eigenvector #3 for 11.1%.

Movie S2. Motions Corresponding to the First Three Eigenvectors from the Multibody Refinement of the PTC18 Dataset. Eigenvector #1 accounts for 29.7% of the total variance in the dataset, eigenvector #2 for 22.5%, and the eigenvector #3 for 14.4%.